


Synthesis, Structures, and Properties of Two Three-Dimensional Metal–Organic Frameworks, Based on Concurrent Ligand Extension

Dabin Shi,^{†,‡} Yanwei Ren,[†] Huanfeng Jiang,^{*,†} Bowei Cai,[†] and Jiaxian Lu[†][†]School of Chemistry and Chemical Engineering, South China University of Technology, Guangzhou 510640, People's Republic of China[‡]School of Pharmaceutical Sciences, Zunyi Medical College, Zunyi 563003, People's Republic of China Supporting Information

ABSTRACT: A tritopic carboxylate ligand, tris(4'-carboxybiphenyl)amine (**L-H₃**), has been synthesized and applied in the construction of microporous metal–organic frameworks (MOFs). Two novel metal–organic frameworks (MOFs), {[Zn₂(**L**)(OH)]·2DMF·H₂O}_∞ (**1**) and {[Cu(**L-H**)(DMA)]·DMA·2H₂O}_∞ (**2**), have been constructed out of **L-H₃**, Zn²⁺, and Cu²⁺, respectively. **1** has a 2-fold interpenetrating three-dimensional framework formed by **L** connectors and the [Zn₂(CO₂)₃] secondary building units (SBUs). As for **1**, it is worth pointing out that one μ₂-OH group links two Zn atoms between two neighboring SBUs to produce interesting Zn–O–Zn zigzag chains in the structure. **2** has a two-dimensional grid sheet formed by **L-H** connectors and the typical paddle-wheel [Cu₂(CO₂)₄] SBUs. Two-dimensional (2D) sheets nest with each other, which finally forms a three-dimensional (3D) nested framework. Two MOFs are characterized by infrared (IR) spectroscopy, thermogravimetry, single-crystal and elemental analyses, and powder X-ray diffraction methods. Framework **1**' exhibits high permanent porosity (Langmuir surface area = 848 m²/g), high thermal stability (up to 450 °C), highly active properties for Friedel–Crafts alkylation reaction, as well as the potential application for the CO₂ gas storage and luminescent material. The catalytic results reveal that **2**' is indeed an efficient heterogeneous catalyst for olefin epoxidation reactions.

1. INTRODUCTION

Metal–organic frameworks (MOFs) have attracted considerable attention, because of their unique properties as permanently microporous materials.^{1–6} To use a virtually unlimited range of organic struts would design diverse structures of MOFs for many applications, such as gas storage,^{7–9} chemical sensing,^{10–12} catalysis,^{13–17} and controlled release of drugs.^{18–20} Currently, the study on MOFs as catalysts is one of the hot topics. Compared with conventional homogeneous catalysts, MOFs as heterogeneous catalysts have many good advantages, including separation and recovery, disposal of spent catalysts, and so on. Moreover, MOFs can be designed as shape-, size-, chemo-, or enantio-selective catalysts. However, reports of catalytic studies in MOFs have been relatively scarce.^{21,22}

MOFs have been investigated for decades; however, a challenge has come from the development of thermally stable porous materials that have permanent porosity. The “node and bridging ligand” approach is important to shape-selective catalysis, because it provides a rational method to build networks with tunable pore size. The strategy for increasing the pore volume and size involves the expansion of known ligands through the use of lengthened but geometrically equivalent organic bridging ligands. Tritopic carboxylate linkers (e.g., 1,3,5-benzenetricarboxylic acid) have been widely used to construct versatile MOFs.^{23,24} For example, Yaghi and co-workers have reported MOF-150, which is composed of the node [Zn₄O(CO₂)₆] and the bridging ligand 4,4',4"-tricarboxytriphenylamine (TCA).²⁵ In most cases, solvothermal reactions of tritopic carboxylate linkers and zinc salts usually produce the [Zn₄O(CO₂)₆] SBUs. As is known to all, the

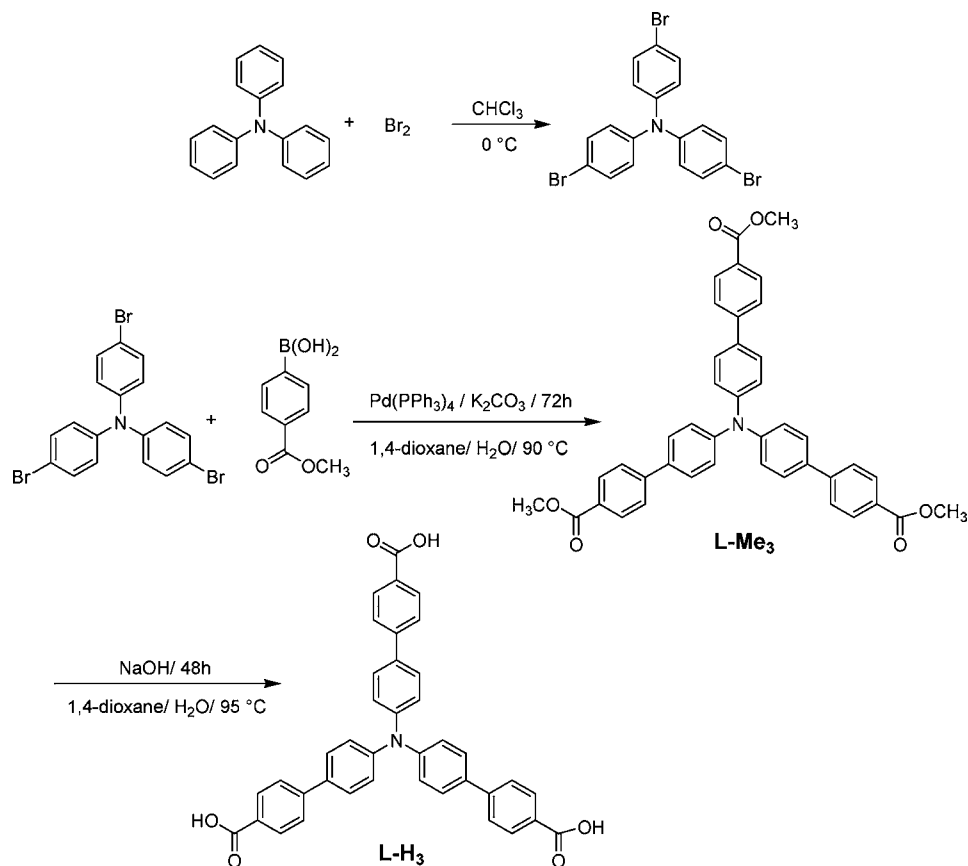
development of rational approaches to the design of MOFs based on elongated tricarboxylic acids is a subject continually attracting interest in inorganic chemistry. To use these elongated ligands has produced many interesting porous MOFs that possess large-sized channels and surface area and shows excellent properties.^{26,27} Herein, we developed a similar ligand **L-H₃** to TCA through concurrent ligand extension, to enhance the channel size and surface area. So far, there has been only one related report to use this ligand to build SNU-77,²⁸ which has a three-dimensional (3D) interpenetrating porous structure formed by the [Zn₄O(CO₂)₆] SBUs and tris(4'-carboxybiphenyl)amine (H₃TCBPA). The authors investigated different fine structures of the SNU-77 in various activation processes, such as room-temperature evacuation, supercritical CO₂ drying, high temperature evacuation, and gas sorption properties.

In this report, tritopic carboxylic acid (**L-H₃**) was used to synthesize two new MOFs. A solvothermal reaction between **L-H₃** and Zn(NO₃)₂·6H₂O in a *N,N*-dimethylformamide (DMF) and H₂O mixture afforded light yellow crystals with a formula of {[Zn₂(**L**)(OH)]·2DMF·H₂O}_∞ (**1**). The other solvothermal reaction between **L-H₃** and Cu(NO₃)₂·3H₂O in a *N,N*-dimethylacetamide (DMA) and H₂O mixture with 15 drops of 3 M HCl produced deep blue crystals with a formula of {[Cu(**L-H**)(DMA)]·DMA·2H₂O}_∞ (**2**). Two formulas were established based on single-crystal X-ray diffraction (XRD) studies, powder X-ray diffraction (PXRD) studies, elemental analysis, and thermogravimetric analysis (TGA) results.

Received: December 6, 2011

Published: June 6, 2012

Scheme 1



Furthermore, we investigated several properties of **1** and **2**, such as adsorption, catalysis, and luminescence. **1** and **2** were activated at $200\text{ }^\circ\text{C}$ for 8 h under vacuum, which gave rise to **1'** and **2'**, respectively. The experimental results reveal that **1'** is a highly efficient catalyst for the Friedel–Crafts alkylation reaction. Moreover, **1** also shows the potential application for the CO_2 gas storage and luminescent material. The olefin epoxidation reactions were carried out using compound **2'** as a catalyst. The catalytic results reveal that **2'** is an excellent heterogeneous Lewis acid catalyst with a high selectivity toward nonterminal olefin.

2. EXPERIMENTAL SECTION

2.1. General Information. All solvents were purchased from Alfa or TCI and used without further purification. Powder X-ray diffraction (PXRD) patterns were collected on a Bruker D8 powder diffractometer at 40 kV, 40 mA with $\text{Cu K}\alpha$ radiation ($\lambda = 1.5406\text{ \AA}$), with a scan speed of 17.7 s/step and a step size of $0.02^\circ (2\theta)$. Thermogravimetric analyses (TGA) were performed on a Q600 SDT instrument under a flow of N_2 at a heating rate of $10\text{ }^\circ\text{C min}^{-1}$ between ambient temperature and $800\text{ }^\circ\text{C}$. Nitrogen and carbon dioxide adsorption experiments were performed with Quantachrome AS-1 MP. Liquid nitrogen was used as coolants to achieve cryogenic temperatures (77 K). The experiments were conducted using ultrahigh-purity N_2 (99.999%), and CO_2 (99.998%). The N_2 sorption isotherms were collected using a pressure range from 10^{-6} atm to 1 atm at 77 K . The CO_2 sorption isotherm was performed at 273 K , using a pressure range of 0.1–1 atm. Elemental analyses for C, H, and N were carried out using a Vario EL III Elemental Analyzer. Room-temperature UV/vis spectra measurements were recorded using quartz cuvettes (1 cm) with Teflon stopper on a U-3100 UV/vis spectrophotometer. Luminescence spectra were recorded at room temperature on a Hitachi F-4500 fluorescence spectrophotometer. ^1H

NMR and ^{13}C NMR were done on a Bruker Model AM-400 (400 MHz) spectrometer. Infrared (IR) spectra were measured from a KBr pellets on a Nicolet Model Nexus 470 FT-IR spectrometer in the range of $4000\text{--}400\text{ cm}^{-1}$. Gas chromatography-mass spectroscopy (GC-MS) spectrometry was recorded on Shimadzu Model GCMS-QP5050A system that was equipped with a $0.25\text{ mm} \times 30\text{ m}$ DB-WAX capillary column.

2.2. Synthesis of Ligand.²⁹ Tris(4'-carboxybiphenyl)amine (**L-H₃**) was synthesized by a Pd-catalyzed Suzuki coupling between tris(4-bromophenyl)amine and 4-(methoxycarbonyl)phenylboronic acid, followed by a base-catalyzed hydrolysis reaction, as shown in Scheme 1.

2.2.1. Synthesis of Tris(4-bromophenyl)amine.³⁰ Triphenylamine (4.78 g, 19.48 mmol) was dissolved in 30 mL of chloroform and cooled to $0\text{ }^\circ\text{C}$ prior to the dropwise addition of bromine (9.27 g, 58 mmol). After complete addition of the bromine, the resulting green solution was stirred for another hour and the crude product was precipitated via the addition of 50 mL of hot ethanol. The product then was allowed to crystallize overnight at $-18\text{ }^\circ\text{C}$, before the precipitate was filtered off and dried under vacuum. Tris(4-bromophenyl)amine (7.54 g, 80%) was obtained as white crystals: mp $143\text{--}144\text{ }^\circ\text{C}$. ^1H NMR (CDCl_3): δ 6.86 (d, $J = 8.8\text{ Hz}$, 6H), 6.93 (d, $J = 8.8\text{ Hz}$, 6H).

2.2.2. Synthesis of Tris(4'-methoxycarbonylbiphenyl)amine (L-Me₃). A mixture of 4-(methoxycarbonyl)phenylboronic acid (3.5 g, 23 mmol, 5.6 equiv), tris(4-bromophenyl)amine (2.0 g, 4.15 mmol), palladium tetrakis(triphenylphosphine) (0.24 g, 0.21 mmol, 5.1 mol %), and potassium carbonate (4.58 g, 33 mmol, 8 equiv) in 100 mL of dioxane/ H_2O (19/1) was stirred under nitrogen for 72 h at $90\text{ }^\circ\text{C}$. After the mixture was cooled to room temperature, it was extracted with CH_2Cl_2 and washed with H_2O several times. The organic layer was then dried with MgSO_4 , and the solvent was removed with a rotary evaporator. The resulting crude product was purified by column chromatography using silica gel and methylene chloride as the eluent.

The product was obtained after removal of the solvents (2.50 g, 93.3% yield). ^1H NMR (CDCl_3): δ 6.86 (d, $J = 8.0$ Hz, 6H); 7.57 (d, $J = 8.0$ Hz, 6H); 7.67 (d, $J = 8.0$ Hz, 6H); 8.10 (d, $J = 8.0$ Hz, 6H); 3.94 (s, 9H). ^{13}C NMR (CDCl_3): δ 52.14, 124.57, 126.5, 128.22, 128.56, 130.18, 131.90, 144.83, 147.29, 166.80. Anal. Calcd (%) for $\text{C}_{42}\text{H}_{33}\text{O}_6\text{N}$: C, 77.88; H, 5.14; N, 2.16; Found: C, 77.69; H, 4.42; N, 2.29.

2.2.3. Synthesis of Tris(4'-carboxybiphenyl)amine (L-H₃). NaOH (15.0 g) was added to a suspension of 2.50 g of tris(4'-carboxymethoxybiphenyl)amine in 130 mL of dioxane/ H_2O (ratio 10/3) and the mixture was stirred under reflux for 48 h at 95 °C. The solvent was removed under vacuum, and then H_2O was added to the residue. The mixture (yellow clear solution) was stirred at room temperature for 2 h. The pH value was adjusted to 2 using concentrated HCl. The resulting yellow solid was collected by filtration, washed with water, HCl (1 M), and diethyl ether, and then dried under vacuum. Yield: 2.23 g, 97%. ^1H NMR ($\text{DMSO}-d_6$): δ 7.22 (d, $J = 8.4$ Hz, 6H); 7.76 (d, $J = 8.8$ Hz, 6H); 7.805 (d, $J = 8.8$ Hz, 6H); 8.01 (d, $J = 8.4$ Hz, 6H). ^{13}C NMR ($\text{DMSO}-d_6$): δ 124.31, 126.23, 128.20, 128.56, 129.96, 133.66, 143.51, 146.77, 167.12. Anal. Calcd (%) for $\text{C}_{39}\text{H}_{27}\text{O}_6\text{N}$: C, 77.34; H, 4.49; N, 2.31; Found: C, 77.25; H, 4.57; N, 2.46.

2.3. Synthesis of $[\{\text{Zn}_2(\text{L})(\text{OH})\} \cdot 2\text{DMF} \cdot \text{H}_2\text{O}]_\infty$ (1). A mixture of L-H₃ (21 mg, 0.033 mmol) and $\text{Zn}(\text{NO}_3)_2 \cdot 6\text{H}_2\text{O}$ (30 mg, 0.13 mmol) was dissolved in a solvent mixture of DMF/ H_2O (4.5 mL/1.5 mL) in a 25-mL Teflon-lined autoclave and heated at 85 °C for one day, then cooled at 5 °C every 1 h to room temperature. Light yellow crystals of a single phase were obtained. The product was isolated by decanting the mother liquor and washing with the mixture of 24 mL of dimethylformamide (DMF) and 8 mL of H_2O (approximately 3×11 mL). The yield of the reaction, determined from the weight of the solvent-free material (18.0 mg), is 56.7% based on L-H₃. Anal. Calcd (%) for $\text{C}_{45}\text{H}_{41}\text{O}_{10}\text{N}_3\text{Zn}_2$: C, 59.06; H, 4.52; N, 4.56; Found: C, 59.12; H, 4.48; N, 4.59. IR data (KBr pellet, ν/cm^{-1}): 3644(m), 3444(s), 2924(m), 1602(s), 1415(s), 1279(s), 806(m), 778(m), 723(m), 489(m). (See Figure S9 in the Supporting Information.)

2.4. Synthesis of $[\{\text{Cu}(\text{L}-\text{H})(\text{DMA})\} \cdot \text{DMA} \cdot 2\text{H}_2\text{O}]_\infty$ (2). A mixture of L-H₃ (18 mg, 0.03 mmol) and $\text{Cu}(\text{NO}_3)_2 \cdot 3\text{H}_2\text{O}$ (31 mg, 0.13 mmol) was dissolved in a solvent mixture of *N,N*-dimethylacetamide and water (DMA/ H_2O , 4.5 mL/1.5 mL) with 15 drops of 3 M HCl (pH ~4) in a vial and heated at 85 °C for two days, then cooled at 5 °C every 1 h to room temperature. Deep blue crystals of a single phase were obtained. The product was isolated by decanting the mother liquor and washing with the mixture of 24 mL of DMA and 8 mL of H_2O (approximate 3×11 mL). The yield of the reaction, determined from the weight of the solvent-free material (21.0 mg), is 71.6% based on L-H₃. Anal. Calcd (%) for $\text{C}_{47}\text{H}_{47}\text{O}_{10}\text{N}_3\text{Cu}$: C, 58.52; H, 4.91; N, 4.36; Found: C, 58.36; H, 4.98; N, 4.52. IR data (KBr pellet, ν/cm^{-1}): 3031(s), 2931(s), 1926(w), 1708(s), 1601(s), 1406(s), 1278(s), 833(m), 778(m), 723(m), 513(m). (See Figure S10 in the Supporting Information.) The experimental results show that a certain amount acid is necessary to synthesize compound 2; subsequently, we performed gradient experiments in the pH value range of 1.0–6.5, and found that the best results are obtained based on pH value between 3.0 to 5.0. As for 1, the addition of acid (e.g., HCl) would give rise to a great quantity of deposits rather than good crystal. Maybe the result is ascribed to the hydrolysis of DMF, because acid can promote the hydrolysis of DMF and produce basic dimethylamine at 85 °C, which is adverse to produce crystal.

2.5. Crystal Structure Determinations. Single-crystal XRD analyses of complexes 1 and 2 were performed on a Rigaku Model Mercury CCD diffractometer operated at 90 kV and 50 mA, using Mo $K\alpha$ radiation ($\lambda = 0.71073$ Å) at room temperature. The empirical absorption corrections were performed using the CrystalClear program.³¹ The structures were solved by direct methods and refined on F^2 by full-matrix least-squares technique using the SHELX-97 program package.³² The single Zn and Cu atoms in the asymmetric unit were located first, followed by the other atoms in the main framework (O, C, and N) from the Fourier difference map. All non-hydrogen atoms were refined with anisotropic displacement

parameters. Hydrogen atoms attached to carbon were placed in geometrically idealized positions and refined using a riding model. The chemical formulas of 1 and 2 were determined using a combination of TGA, elemental analysis, and single-crystal XRD studies. Cambridge Crystallographic Data Centre files CCDC 870429 and 854187 contain the supplementary crystallographic data for this paper. (These data can be obtained free of charge from The Cambridge Crystallographic Data Centre via www.ccdc.cam.ac.uk/data_request/cif.)

Crystallographic Data for 1. Orthorhombic, space group: *Pcca*, $a = 11.980(2)$ Å, $b = 18.625(4)$ Å, $c = 17.982(4)$ Å, $V = 4012.4(14)$ Å³, $Z = 4$, $\rho_{\text{calcd}} = 1.484$ g cm⁻³, $\mu(\text{Mo } K\alpha) = 1.257$ mm⁻¹, data/restraints/parameters: 4602/0/272, $R_1(I > 2s(I)) = 0.0451$, $wR_2 = 0.1302$, $R_1(\text{all data}) = 0.0571$, $wR_2(\text{all data}) = 0.1382$, goodness of fit (GOF) = 1.042. (CCDC File No. 870429.)

Crystallographic Data for 2. Monoclinic, space group: *P2₁/c*, $a = 18.023(4)$ Å, $b = 18.952(4)$ Å, $c = 12.389(3)$ Å, $\beta = 90.8364^\circ$, $V = 4231.0(15)$ Å³, $Z = 4$, $\rho_{\text{calcd}} = 1.321$ g cm⁻³, $\mu(\text{Mo } K\alpha) = 1.266$ mm⁻¹, data/restraints/parameters: 7217/64/538, $R_1(I > 2s(I)) = 0.0868$, $wR_2 = 0.2313$, $R_1(\text{all data}) = 0.1466$, $wR_2(\text{all data}) = 0.2749$, GOF = 0.998. (CCDC File No. 854187.)

2.6. Catalytic Experiments. **2.6.1. Friedel–Crafts Alkylation Reaction.** The liquid-phase alkylation reaction of toluene with benzyl bromide was carried out in a magnetically stirred glass reactor (50 mL) fitted with a reflux condenser. 1 was activated at 200 °C for 8 h under vacuum before the reaction was carried out. Typically, a mixture of benzyl bromide (2.5 mmol), 1' (0.021 g, 0.125 mmol), and 10 mL of toluene was heated at 100 °C for 10 h. After cooled to room temperature, the mixture was then filtered and the filtrate was analyzed with gas chromatography–mass spectrometry (GC-MS) (using 1,3,5-trimethylbenzene as an internal standard). In addition, the solvent (excessive toluene) was removed with a rotary evaporator. The resulting crude product was quantified by ^1H NMR spectroscopic methods, using cyclohexane as an internal standard.

2.6.2. Olefin Epoxidation Reaction. 2 was activated at 200 °C for 8 h under vacuum before the reaction was carried out. The oxidation of olefin was carried out in a 20-mL test tube at atmospheric pressure and 60 °C, using acetonitrile as a solvent (5 mL). Typically, A 0.01 mmol (1%) portion of the catalyst 2' was stirred in a suspension containing the solvent and 1.0 mmol of the olefin. The oxidant (*t*-BuOOH, 2.5 mmol, 2.5 equiv) was added dropwise, while the overall suspension was heated to 60 °C. The reaction mixture was stirred continuously for 24 h. After cooled to room temperature, the product was then filtered and the filtrate was analyzed with GC-MS (using 1,3,5-trimethylbenzene as an internal standard). At the same time, the epoxide was confirmed by ^1H NMR. Typically, the mixture was filtered after reaction, and the solvent was removed with a rotary evaporator. The resulting crude product was purified by column chromatography using silica gel and petroleum ether/ethyl acetate (9/1) as the eluent. The product was obtained after removal of the solvents.

Phenyloxirane: ^1H NMR (400 MHz, CDCl_3): δ 2.79–2.80 (m, 1 H), 3.12–3.13 (m, 1 H), 3.85–3.86 (m, 1 H), 7.28–7.34 (m, 5 H). **cis-stilbene oxide:** ^1H NMR (400 MHz, CDCl_3): δ 3.91 (s, 2 H), 7.23–7.41 (m, 10 H). **1,2-epoxycyclooctane:** ^1H NMR (400 MHz, CDCl_3): δ 1.24–1.31 (m, 4 H), 1.41–1.62 (m, 4 H), 2.09–2.18 (m, 4 H), 2.83–2.94 (m, 2 H). **4-tert-butylstyrene oxide:** ^1H NMR (400 MHz, CDCl_3): δ 1.21 (s, 9 H), 2.78–2.80 (m, 1 H), 3.11–3.12 (m, 1 H), 3.85–3.86 (m, 1 H), 7.11(d, $J = 8.4$ Hz, 2 H), 7.23(d, $J = 8.4$ Hz, 2 H). **1,2-Epoxyhexane:** ^1H NMR (400 MHz, CDCl_3): δ 0.92(t, $J = 14.1$ Hz, 3 H), 1.38–1.40 (m, 4H), 1.53–1.54 (m, 2H), 2.46–2.47 (m, 1H), 2.74–2.75 (m, 1 H), 2.9 (m, 1H).

3. RESULTS AND DISCUSSION

3.1. Crystal Structures. Single-crystal X-ray structure determination of 1 reveals a 2-fold interpenetrating three-dimensional (3D) framework that crystallizes in orthorhombic space group *Pcca*. Each asymmetric unit contains one-half of the L ligands, one Zn atom, and one bridging OH group. The Zn atom coordinates to three different carboxylate oxygen atoms of the L ligand in the equatorial positions to form the

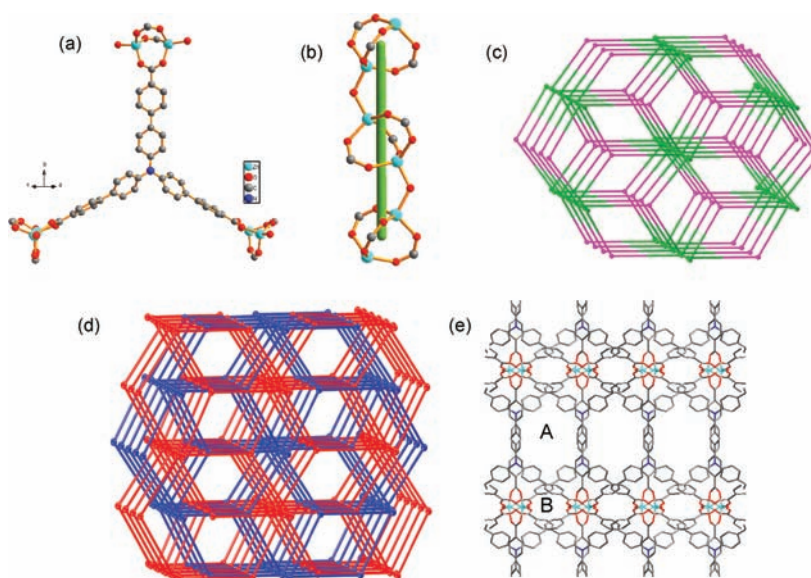


Figure 1. (a) Representation of coordination modes of Zn and L ligand, (b) chain structure of hydroxy group links Zn atom between two SBUs, (c) 3-connected 3D net of **1**, (d) 2-fold interpenetrating 3D net of **1**, (e) stick models of **1** as viewed along the *a*-axis with 9.4 Å × 9.8 Å (A) and 4.7 Å × 5.5 Å (B) channels. Zn (light blue), carbon (gray), nitrogen (deep blue), and oxygen (red). Hydrogen atoms are omitted for clarity.

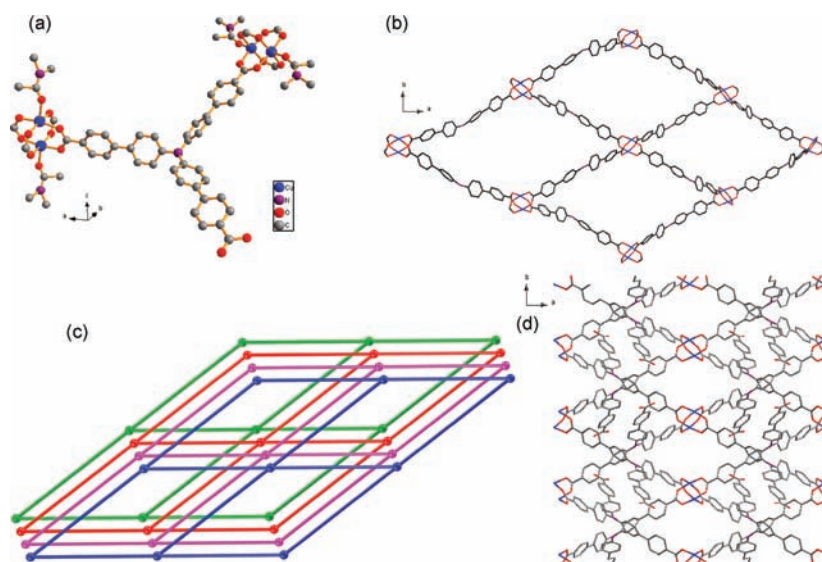


Figure 2. (a) Representation of coordination modes of Cu and L-H, (b) 4-connected net of **2**, (c) 3D nest net of **2**, (d) stick models of **2** as viewed along the *c*-axis without DMA. Cu (deep blue), carbon (gray), nitrogen (purple), and oxygen (red). Hydrogen atoms are omitted for clarity.

[Zn₂(CO₂)₃] SBUs (Figure 1a). The central Zn(II) ion is four-coordinated by three O atoms and one OH group O-donor (Zn–O = 1.961–1.930 Å; Zn–OH = 1.908 Å). Each unit cell contains one complete L ligand and two [Zn₂(CO₂)₃] SBUs, with OH group binding to the axial positions, giving the framework formula of [Zn₂(L)(OH)]. It is worth pointing out that one μ₂–OH group links two Zn atoms between two neighboring SBUs to produce Zn–O–Zn zigzag chains (Figure 1b). The Zn–Zn distance and Zn–O–Zn angle between two SBUs are 3.369 Å and 123.91°, respectively. There has been a small amount of literature to report such structures.³³ The ligand links the [Zn₂(CO₂)₃] SBUs and one OH links two Zn atoms between two neighboring SBUs, which forms a 2-fold self-penetrating 3D framework (see Figure 1d). The topology of **1** assumes that the trigonal L ligand keeps its 3-connectivity and each Zn₂(CO₂)₃ SBUs acts as a 5-connected node. The

resulting 3,5-connected net has a vertex symbol (6².8)-(6⁶.8².10²) (see Figure 1c).

Compound **1** has open channels along the *a* or *c* crystallographic direction, with two channel openings of 9.4 Å × 9.8 Å (using PLATON³⁴ software to measure the distance between atom centers) and 4.7 Å × 5.5 Å along the *a*-axis (see Figure 1e) and one channel opening of 12.4 Å × 3.9 Å along the *c*-axis. (See Figure S2 in the Supporting Information.) PLATON calculations³⁴ of **1** indicated a void volume of 1131.5 Å³ (28.0% of the unit cell volume of 4012.4 Å³) that is filled with 2 DMF molecules and 1 water molecule. Consistent with this finding, the TGA analysis of **1** showed a solvent weight loss of 18.0% in the 50–300 °C temperature range (calc. 17.9%).

Single-crystal XRD reveals that **2** crystallizes in monoclinic space group *P*2₁/*c*. The asymmetric unit consists of one copper ion, one L-H ligand, and one coordinated *N,N*-dimethylaceta-

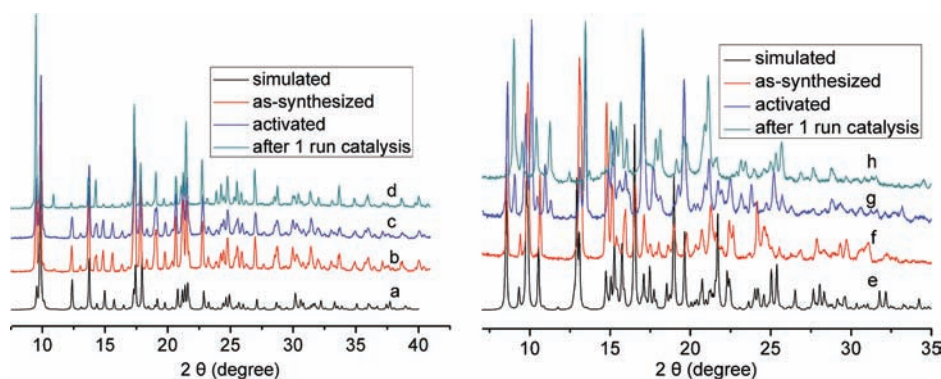


Figure 3. Powder X-ray diffraction (PXRD) patterns of **1** and **2**: (a) **1** simulated patterns from single-crystal structure, (b) **1** as-synthesized pristine sample, (c) **1'** (**1** activated sample at 200 °C for 8 h), (d) **1'** after a one-run catalysis recycle, (e) **2** simulated patterns from single-crystal structure, (f) **2** as-synthesized pristine sample, (g) **2'** (**2** activated sample at 200 °C for 8 h), and (h) **2'** after a one-run catalysis recycle.

amide (DMA) molecule (see Figure 2a). The central Cu(II) ion is five-coordinated by four oxygen atoms ($d(\text{Cu}-\text{O}) = 1.936\text{--}1.956 \text{ \AA}$) from four different L-H ligands in a square-pyramidal geometry and one DMA O-donor ($d(\text{Cu}-\text{O}) = 2.136 \text{ \AA}$). Four carboxylate groups from different ligands connect a pair of Cu ions to generate the paddlewheel units $[\text{Cu}_2(\text{CO}_2)_4]$ (Cu...Cu distance of 2.6507 Å), in which the axial positions are occupied by DMA O-donors. One carboxyl group of L-H₃ is not ionized and therefore does not serve as a donor to coordinate the Cu atom. It only forms intermolecular hydrogen bonds ($d(\text{D}\cdots\text{A}) = 2.645 \text{ \AA}$; $d(\text{H}\cdots\text{A}) = 1.866 \text{ \AA}$) with one guest DMA molecule filling in the channels. The L-H ligands link the $[\text{Cu}_2(\text{CO}_2)_4]$ SBUs and two DMA molecules link two Cu atoms, respectively, which forms a two-dimensional (2D) grid sheet (see Figure 2b). The assembly of linear ditopic carboxylate ligands with paddlewheel SBUs usually generates default 2D grid sheet structures. 2D sheets nest within each other, which finally forms a 3D framework (see Figure 2c). Obviously, there is a one-dimensional (1D) channel along the *c* crystallographic direction (Figure 2d) after the removal of coordinated DMA and guest molecules. The topology of **2** assumes that the L-H ligand keeps its 2-connectivity and each $\text{Cu}_2(\text{CO}_2)_4$ SBUs acts as a 4-connected node. The resulting net has a vertex symbol ($4^4.6^2$) (see Figure 2c).

3.2. Thermogravimetric Analysis (TGA) and Powder X-ray Diffraction (PXRD) Analyses. Thermogravimetric analysis (TGA) was carried out to examine the stability of the framework **1** and **2**. The TGA curve of **1** shows a weight loss of 18.0% from 50 °C to 300 °C, corresponding to the loss of disordered waters and DMF molecules in the channels (calc. 17.9%) and then an intense weight loss from ~450 °C, which is attributed to the decomposition of the framework and ended after 500 °C to give a total weight loss of ~60.0% (see Figure S4 in the Supporting Information). TGA curve of **2** shows a weight loss of ~24.0% from room temperature to 330 °C, corresponding to the loss of coordinated DMA, uncoordinated DMA, and disordered water molecules (calc. 23.96%) (see Figure S4 in the Supporting Information).

The pure compounds **1** and **2** were confirmed by PXRD measurement in which the diffraction peaks of experimental data are in excellent agreement with the simulated data from single-crystal X-ray data (see Figures 3b and 3f). We then performed the PXRD measurement of **1'** and **2'**, respectively (see Figures 3c and 3g). As far as **1'** is concerned, the results still match very well with simulated data, indicating no obvious structural change, which demonstrates that **1** possesses

permanently stable microporosity. As for **2'**, slight differences are observed between 5° and 20° by comparing the X-ray diffractograms of **2** and **2'**, which indicates that the crystalline structure of the material is preserved. The slight differences might result from the removal of coordinated DMA molecules.

3.3. Gas Sorption. We have determined the permanent porosity of **1'** by nitrogen adsorption at 77 K, as well as the carbon dioxide uptake capacity at 273 K. The N₂ adsorption isotherm of **1'** reveals Type I behavior, indicative of microporous materials (see Figure 4). The nitrogen adsorption

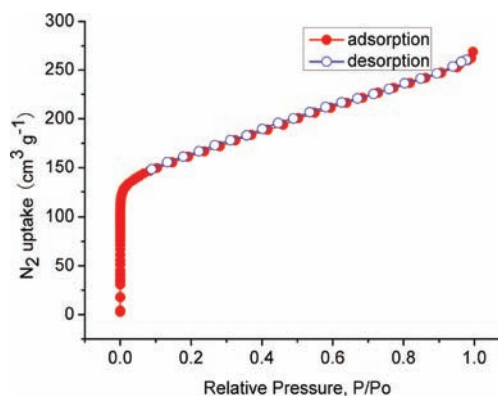


Figure 4. Nitrogen adsorption isotherm of **1'** at 77 K (solid red circles, adsorption; open blue circles, desorption).

shows good reversibility. From these data, the apparent surface area was calculated using the Langmuir method to be 848 m²/g (588 m²/g BET), thus confirming the permanent porosity of **1'**. The CO₂ gas adsorption property of **1'** was investigated. The result shows that CO₂ uptake is ~42.0 cm³/g at 273 K at 1.0 atm, highlighting its potential application for the CO₂ gas storage (see Figure 5). In contrast, its carbon dioxide uptake is moderate.³⁵

3.4. Fluorescent Properties. The ultraviolet–visible light (UV/vis) spectra properties of L-H₃ and **1** were investigated at room temperature. The L-H₃ sodium salt aqueous solution (1.0 × 10⁻⁵ M) displays strong absorption bands in the UV spectral region from 200 nm to 400 nm, in which the absorbance maxima is 255 nm and 360 nm, which are attributed to the *n*-π* and π-π* transition of the aromatic rings, respectively. While the absorbance maxima of **1** in the solid state is 357 nm. Subsequently, the fluorescent properties of L-H₃ and **1** were also investigated at room temperature. The excitation wave-

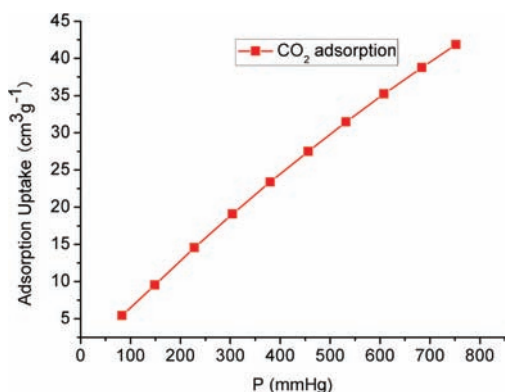


Figure 5. Carbon dioxide adsorption isotherms at 273 K for **1'**.

length of 360 nm was set from the absorption maximum determined from the UV/vis spectral data. The **L-Na₃** fluoresces in aqueous solution (1.0×10^{-5} M) with an emission maximum at 507 nm, whereas **1** in the solid state displays an emission maximum at 480 nm. A blue shift of 27 nm in the emission spectrum was observed. **2** in the solid state is nonemissive, because of luminescence quenching by the d–d transition of the Cu²⁺. The results indicate that **1** and **L** possess blue and green fluorescence properties, respectively. (See Figures S5–S8 in the Supporting Information.)

3.5. Catalytic Properties. Friedel–Crafts alkylation is one of the most efficient methods for the derivatization of aromatic compounds.³⁶ The use of heterogeneous catalysts in the liquid phase is highly desirable for the Friedel–Crafts alkylation reaction,^{37–40} because the use of conventional homogeneous catalysts for this reaction would lead to several problems, such as difficulty in separation and recovery and disposal of spent catalysts. In the light of the importance of heterogeneous catalysis, Friedel–Crafts alkylation reactions, in which **1'** was used as a promising heterogeneous catalyst, have been investigated. **1** was activated at 200 °C for 8 h under vacuum before the reaction. Friedel–Crafts alkylation reactions of toluene with several benzyl bromide containing different substituent groups were performed at 100 °C for 10 h, such as benzyl bromide (BB), 4-nitrobenzyl bromide (NBB), and 3,5-di-*tert*-butylbenzyl bromide (TBBB). The results were summarized in Table 1. No conversion was observed when the reaction was performed without compound **1'** or using **2'** as a catalyst. When as-synthesized pristine sample **1** and anhydrous ZnCl₂ are used as catalysts, the conversion of BB is 8.2% and 99%, respectively, with 4.8% and 96.1% total yield, respectively. Under standard reaction conditions, the experimental results demonstrate that **1'** is an excellent catalyst for BB and NBB conversion (>99%) with 97.2% and 94.5% total yield, respectively. (See Figure S11 in the Supporting Information.) With the size extension of the substrates, the conversion of TBBB drops to 98.2% with a 91.8% total yield. (See Figure S12 in the Supporting Information.) A slight degradation of the conversion suggests that large substrates are difficult to enter into the channels, relative to small ones. It must be noted that all alkylation products are composed of *o*-isomer and *p*-isomer (see Figures S11 and S12 in the Supporting Information), which is similar to the results reported by this literature.^{38–40} Several authors have reported different results in the Friedel–Crafts alkylation reactions using MOFs that contained Zn²⁺ as catalysts. Phan and co-workers have performed the Friedel–Crafts alkylation reactions of

Table 1. Friedel–Crafts Alkylation Reactions of Toluene with Various Reactant Substrates Catalyzed by Compound **1'**^a

entry	substrates	conversion (%) ^b	yield (%) ^c
1 ^d		0	0
2 ^e		0	0
3 ^f		8.2	4.8
4 ^g		>99	96.1
5		>99	97.2
6		>99	94.5
7		98.2	91.8

^aConditions: a mixture of benzyl bromide (2.5 mmol), **1'** (0.125 mmol) and 10 mL of toluene was stirred at 100 °C for 10 h. ^bDetermined by GC-MS (using 1,3,5-trimethylbenzene as an internal standard). ^cDetermined by ¹H NMR (using cyclohexane as an internal standard). ^dWithout **1'**. ^eUsing **2** as catalyst. ^fUsing as-synthesized pristine sample **1** as catalyst. ^gUsing anhydrous ZnCl₂ as catalyst.

toluene with benzyl bromide using MOF-5 as a catalyst at 80 °C for 4 h.³⁸ As far as our work is concerned, in contrast, although the total reaction conversion rates (99%) are on par with theirs, reaction time (10 h) is longer than 4 h and reaction temperature (100 °C) is slightly higher than 80 °C, respectively. One possible reason is that the MOF-5 catalyst can present more active centers, relative to **1'**. He and co-workers⁴¹ have also successfully used ZnPC-2 to catalyze the Friedel–Crafts alkylation reaction at 110 °C for 18 h. Obviously, we present a shorter reaction time (10 h) and lower reaction temperature (100 °C) in our work than those reported by the authors.

In order to investigate the recyclability of **1'**, Friedel–Crafts alkylation reaction of toluene with benzyl bromide (BB) was performed under the same reaction conditions as described above, except using the recovered catalyst. Each time, the catalyst was isolated from the reaction solution at the end of catalytic reaction, and then dried at 200 °C for 8 h under vacuum. The dried catalyst was then reused in a next run. After a run, the conversion of BB decreases to 85.6%, with 82.5% total yield. It was apparent that compound **1'** could be an alternative to other solid acid catalysts, exhibiting advantages over conventional Lewis acid catalysts such as ZnCl₂ in the Friedel–Crafts alkylation reaction. To better understand the thermal stability of the catalyst after the reaction, PXRD measurement was conducted on the catalyst after a run recycle by filtration (Figure 4d). As shown in Figure 4d, there are slight differences in the peak positions as well as intensities between 5° and 20° by comparing the X-ray diffractograms of the fresh and used catalysts, which indicates that the crystalline structure

Table 2. Epoxidation of Olefins Catalyzed by 2^{aa}

entry	substrates	reaction time(h)	conversion ^b (wt.-%)	yield of products (%)	
				epoxide ^c	other oxide
1 ^d		24	5	trace	5
2 ^e		24	96.2	trace	96.2
3 ^f		24	7.6	trace	7.6
4		24	89.0	48.5	38.2
5		24	94.0	82.0	<5
6		24	98.0	91.0	<1
7		24	94.4	65.7	22.7
8		24	85.1	46.0	39.2

^aConditions: a mixture of olefin (1.0 mmol), 2' (0.01 mmol) and *t*-BuOOH (2.5 mmol) in acetonitrile (5 mL) was stirred at 60 °C for 24 h.

^bDetermined by GC-MS (using 1,3,5-trimethylbenzene as an internal standard). ^cIsolated yield. ^dWithout 2'. ^eUsing Cu(NO₃)₂·3H₂O as catalyst.

^fUsing as-synthesized pristine sample 2 as catalyst.

of the material is partially changed. Atomic absorption spectrophotometry (AAS) analysis of the filtrate after the removal of the catalyst after reaction confirms that the Zn²⁺ content is 1.3 mg/L, indicating that a leaching of 1' slightly occurs during the reaction. A further experiment was carried out to check for the possible occurrence of any leaching. First, after a standard reaction had taken place for 5 h, the mother liquor was split into two fractions: one had the solid catalyst and the other was without the solid catalyst. In this case, the conversion of BB is 62%. After an additional 5 h, the conversion of two fractions is up to 99% (with the solid catalyst) and 78% (without), respectively. The result indicates that 1' acts as a highly active catalyst in these reactions. At the same time, it might still be possible that a small amount of 1' is decomposed in situ during the reaction. A possible mechanism, according to previous literature,^{37–45} is that active centers may arise either from four-coordinated zinc hydroxide clusters or from structural Zn–OH defects formed at the synthesis step.

Olefin epoxidation reactions catalyzed by various metal salts under homogeneous or heterogeneous conditions were extensively documented.^{46,47} However, reports of olefin epoxidation reactions related to heterogeneous catalytic studies on MOFs containing metal copper have been extremely scarce.⁴⁸ Thus, olefin epoxidation reactions, in which 2' acts as a desirable heterogeneous catalyst, have been investigated. As far as 2 is concerned, as coordinated DMA molecules are removed, the Cu active sites are completely exposed in the 1D channels along the *c* crystallographic direction (see Figure 2d), which is similar to the Cu₃(BTC)₂ catalyst.⁴⁹ In order to confirm the removal of coordinated DMA molecules, an as-synthesized pristine sample 2 (0.1821 g) of accurate weight was evacuated at 200 °C for 8 h. 2' (0.1388 g) was obtained. The result shows a weight loss of 2 (0.0433 g), corresponding to 23.7% of pristine sample, in accordance with TGA results. 2 was activated at 200 °C for 8 h under vacuum, to remove

coordinated DMA molecules before the reaction. Olefin epoxidation reactions using *t*-BuOOH as an oxidant were performed at 60 °C for 24 h. The results of the catalytic epoxidation of different substrates were summarized in Table 2. In all cases, blank tests performed under identical conditions gave negligible conversion (5%) of the substrates. Using Cu(NO₃)₂·3H₂O would give a high conversion (96.2%), while the products are almost all benzaldehyde, rather than the epoxide. The result should be attributed to the Lewis acidity of Cu(NO₃)₂·3H₂O, which might be stronger than that of 2'. Under standard reaction conditions, the oxidation of styrene occurs with 89% conversion, while the epoxide yield is 48.5%, and, along with styrene oxide, benzaldehyde is also formed (see Figure S13 in the Supporting Information). Compared with other reports in which *t*-BuOOH served as an oxidant, the reaction has more high selectivity and yield.⁵⁰ In addition, Cao and co-workers have reported that one-dimensional (1D) homochiral nickel coordination polymers can catalyze the oxidation of styrene, because, using *t*-BuOOH as an oxidant, the conversion and selectivity are 33% and 27%, respectively.⁵¹ In contrast, the conversion and selectivity are up to 89.0% and 48.5% in our work, respectively. Maybe the result should be attributed to the catalytic activity of 2', which is higher than that of 1D homochiral nickel coordination polymers. Using as-synthesized pristine sample 2 as the catalyst, the conversion of styrene decreases to 7.6%, indicating that unactivated 2 does not play a catalyst role in the olefin epoxidation reaction. Oxidation of nonterminal olefin, such as *cis*-stilbene and cyclooctene, occurs with 94% and 98% conversion, respectively, while epoxide yields are 82% and 91%, respectively. (See Figure S14 in the Supporting Information.) Obviously, the reaction has remarkable selectivity, based on nonterminal olefin. The epoxide yield of 4-*tert*-butylstyrene is highest up to 65.7%. Maybe electron-donating groups (such as *tert*-butyl) contribute to the epoxide conversion. Oxidation of aliphatic 1-hexene

occurs with 85.1% conversion, while the epoxide yield is 46%. These studies indicate that the oxide conversion rates are desirable based on different substrates, while the epoxide yields are obviously different. Usually, oxidation of olefin gives different products, such as aldehyde, ketone, epoxide, etc.⁵² As far as nonterminal olefin oxidation is concerned, the reaction presents high selectivity and the epoxide is one of the primary products,⁵³ which is attributed to the fact that the epoxide based on nonterminal olefin is more stable, relative to those based on terminal olefin, and the former is more unlikely to incur further oxidation than the latter.

The recyclability of catalyst **2'** was examined on the epoxidation of styrene. After the epoxidation reaction, the catalyst was separated from the reaction mixture by centrifugation, thoroughly washed with acetone, and then reused as catalyst for the next run under the same conditions. The catalytic results demonstrate that the conversion of styrene decreases to 81.6%, with 42.5% epoxide conversion. In order to confirm the stability of **2**, PXRD measurement was conducted on the catalyst after a run recycle experiment (see Figure 4h). The result shows that no significant differences are observed between the diffractograms, indicating that the crystalline structure of **2** is preserved. Atomic absorption spectrophotometry (AAS) analysis of the filtrate, after the removal of the catalyst after reaction, confirms that the Cu²⁺ content is 0.05 mg/L, indicating the leaching of Cu²⁺ into the solvent was negligible during the reaction. Lastly, an experiment was carried out to check for the possible occurrence of any leaching. First, after a standard reaction have taken place for 12 h, the mother liquor was split into two fractions, in which one had the solid catalyst while the other was without the solid catalyst. In this case, the conversion of styrene is 68%. After an additional 12 h, the conversion rates of two fractions are 86.2% (with the solid catalyst) and 69.4% (without), respectively. The results indicate that **2'** has good stability. Moreover, the solid catalysts still maintain a deep blue color after reaction, which proves that the metal ion coordination sphere is not destroyed. From above studies, we draw a conclusion that **2'** acts as a heterogeneous Lewis acid catalyst in these epoxidation reactions. A plausible mechanism of these olefin epoxidation reactions is that unsaturated Cu acts as Lewis acid catalyst after coordinated DMA molecules are removed.^{54,55}

4. CONCLUSIONS

In summary, we have successfully synthesized a multidentate tricarboxylic acid (L-H₃) through concurrent ligand extension and incorporated it into compound {[Zn₂(L)-(OH)]·2DMF·H₂O}_∞ (**1**) and {[Cu(L-H)-(DMA)]·DMA·2H₂O}_∞ (**2**). **1** and **2** have three-dimensional (3D) novel structures and show good properties. As for **1**, it is worth noting that one μ₂-OH group links two Zn atoms between two neighboring SBUs to produce unusual Zn-O-Zn zigzag chains in the structure. **1'** shows highly active properties for Friedel-Crafts alkylation reaction, which are due to the regular porosities. Furthermore, **1'** possesses promising application for the CO₂ gas storage and luminescent material. **2** is constructed from two-dimensional (2D) grid sheets via interdigitation. **2'** demonstrates an excellent activity and selectivity for olefin epoxidation reactions. To the best of our knowledge, it is the first report that olefin epoxidation reactions were performed using *t*-BuOOH as an oxidant as well as metal-organic frameworks (MOFs) that contain Cu²⁺ as a catalyst. We draw the conclusion that the method to extend ligands could

not only effectively construct MOFs with large size channel and high surface area, but also achieve multifunctional materials with special catalysis.

■ ASSOCIATED CONTENT

Supporting Information

TG, GC-MS, ¹H NMR, IR spectra, luminescence spectra, UV-vis spectra, and supplementary figures. This material is available free of charge via the Internet at <http://pubs.acs.org>.

■ AUTHOR INFORMATION

Corresponding Author

*Fax: +86-20-22236337. E-mail: jianghf@scut.edu.cn.

Funding

The authors declare no competing financial interest.

Notes

The authors declare no competing financial interest.

■ ACKNOWLEDGMENTS

We are grateful to the National Natural Science Foundation of China (Nos. 20932002 and 21172076), the National Basic Research Program of China (973 Program) (No. 2011CB808600), the Natural Science Foundation of Guangdong Province, China (No. 10351064101000000), and the Fundamental Research Funds for the Central Universities (No. 2010ZP0003) for the financial support. We thank Prof. M. L. Tong of Sun Yat-Sen University for his valuable help.

■ REFERENCES

- (1) Zhao, D.; Timmons, D. J.; Yuan, D. Q.; Zhou, H.-C. *Acc. Chem. Res.* **2011**, *44*, 123–133.
- (2) Lee, J. Y.; Farha, O. K.; Roberts, J.; Scheidt, K. A.; Nguyen, S. T.; Hupp, J. T. *Chem. Soc. Rev.* **2009**, *38*, 1450–1459.
- (3) Farrusseng, D.; Aguado, S.; Pinel, C. *Angew. Chem., Int. Ed.* **2009**, *48*, 7502–7513.
- (4) Yoon, M.; Srirambalaji, R.; Kim, K. *Chem. Rev.* **2012**, *112*, 1196–1231.
- (5) Yin, Z.; Wang, Q.-X.; Zeng, M.-H. *J. Am. Chem. Soc.* **2012**, *134*, 4857–4863.
- (6) Zeng, M.-H.; Wang, Q.-X.; Tan, Y.-X.; Hu, S.; Zhao, H.-X.; Long, L.-S.; Kurmoo, M. *J. Am. Chem. Soc.* **2010**, *132*, 2561–2563.
- (7) Bloch, E. D.; Britt, D.; Lee, C.; Doonan, C. J.; Uribe-Romo, F. J.; Furukawa, H.; Long, J. R.; Yaghi, O. M. *J. Am. Chem. Soc.* **2010**, *132*, 14382–14384.
- (8) Dincă, M.; Long, J. R. *Angew. Chem., Int. Ed.* **2008**, *47*, 6766–6779.
- (9) Yang, S.; Martin, G. S. B.; Titman, J. J.; Blake, A. J.; Allan, D. R.; Champness, N. R.; Schröder, M. *Inorg. Chem.* **2011**, *50*, 9374–9384.
- (10) Chen, H.; Wang, L.; Xiao, Y.; Fronczek, F. R.; Xue, M.; Cui, Y.; Qian, G. *Angew. Chem., Int. Ed.* **2009**, *48*, 500–503.
- (11) Pramanik, S.; Zheng, C.; Zhang, X.; Emge, T. J.; Li, J. *J. Am. Chem. Soc.* **2011**, *133*, 4153–4155.
- (12) Allendorf, M. D.; Houk, R. J. T.; Andruszkiewicz, L.; Talin, A. A.; Pikarsky, J.; Choudhury, A.; Gall, K. A.; Hesketh, P. J. *J. Am. Chem. Soc.* **2008**, *130*, 14404–14405.
- (13) Dang, D.; Bai, Y.; He, C.; Wang, J.; Duan, C.; Niu, J. *Inorg. Chem.* **2010**, *49*, 1280–1282.
- (14) Ma, L.; Wu, C.-D.; Wanderley, M. M.; Lin, W. *Angew. Chem., Int. Ed.* **2010**, *49*, 8244–8248.
- (15) Liao, T.-B.; Ling, Y.; Chen, Z.-X.; Zhou, Y.-M.; Weng, L.-H. *Chem. Commun.* **2010**, *46*, 1100–1102.
- (16) Banerjee, M.; Das, S.; Yoon, M.; Choi, H. J.; Hyun, M. H.; Park, S. M.; Seo, G.; Kim, K. *J. Am. Chem. Soc.* **2009**, *131*, 7524–7525.
- (17) Thallapally, P. K.; Fernandez, C. A.; Motkuri, R. K.; Nune, S. K.; Liu, J.; Peden, C. H. F. *Dalton Trans.* **2010**, *39*, 1692–1694.

- (18) Horcajada, P.; Serre, C.; Maurin, G.; Ramsahye, N. A.; Balas, F.; Vallet-Regí, M.; Sebban, M.; Taulelle, T.; Férey, G. *J. Am. Chem. Soc.* **2008**, *130*, 6774–6780.
- (19) Rieter, W. J.; Pott, K. M.; Taylor, K. M. L.; Lin, W. *J. Am. Chem. Soc.* **2008**, *130*, 11584–11585.
- (20) Taylor-Pashow, K. M. L.; Rocca, J. D.; Xie, Z.; Tran, S.; Lin, W. *J. Am. Chem. Soc.* **2009**, *131*, 14261–14263.
- (21) Horike, S.; Dincă, M.; Tamaki, K.; Long, J. R. *J. Am. Chem. Soc.* **2008**, *130*, 5854–5855.
- (22) Shultz, A. M.; Farha, O. K.; Hupp, J. T.; Nguyen, S. T. *J. Am. Chem. Soc.* **2009**, *131*, 4204–4205.
- (23) Chui, S. S. Y.; Lo, S. M. F.; Charmant, J. P. H.; Orpen, A. G.; Williams, I. D. *Science* **1999**, *283*, 1148–1150.
- (24) Zhao, X.; He, H.; Hu, T.; Dai, F.; Sun, D. *Inorg. Chem.* **2009**, *48*, 8057–8059.
- (25) Chae, H. K.; Kim, J.; Friedrichs, O. D.; O’Keeffe, M.; Yaghi, O. M. *Angew. Chem., Int. Ed.* **2003**, *42*, 3907–3909.
- (26) Furukawa, H.; Ko, N.; Go, Y. B.; Aratani, N.; Choi, S. B.; Choi, E.; Yazaydin, A. Ö.; Snurr, R. Q.; O’Keeffe, M.; Kim, J.; Yaghi, O. M. *Science* **2010**, *329*, 424–428.
- (27) Sun, D.; Ke, Y.; Mattox, T. M.; Parkin, S.; Zhou, H. C. *Inorg. Chem.* **2006**, *45*, 7566–7568.
- (28) Park, H. J.; Lim, D. W.; Yang, W. S.; Oh, T. R.; Suh, M. P. *Chem.—Eur. J.* **2011**, *17*, 7251–7260.
- (29) Ma, L.; Jin, A.; Xie, Z.; Lin, W. *Angew. Chem., Int. Ed.* **2009**, *48*, 9905–9908.
- (30) Cremer, J.; Bäuerle, P. *J. Mater. Chem.* **2006**, *16*, 874–884.
- (31) (a) Molecular Structure Corporation. *CrystalClear, Version 1.36*; Molecular Structure Corporation (MSC), The Woodlands, TX, USA, 2000. (b) Rigaku Corporation. *CrystalClear, Version 1.36*; Rigaku Corporation, Tokyo, Japan, 2000.
- (32) Sheldrick, G. M. *Acta Crystallogr., Sect. A: Found. Crystallogr.* **2008**, *A64*, 112–122.
- (33) Rosi, N. L.; Eddaoudi, M.; Kim, J.; O’Keeffe, M.; Yaghi, O. M. *Angew. Chem., Int. Ed.* **2002**, *41*, 284–287.
- (34) Spek, A. L. *J. Appl. Crystallogr.* **2003**, *36*, 7–13.
- (35) Hu, T.-L.; Tao, Y.; Chang, Z.; Bu, X.-H. *Inorg. Chem.* **2011**, *50*, 10994–11003.
- (36) Terada, M.; Sorimachi, K. *J. Am. Chem. Soc.* **2007**, *129*, 292–293.
- (37) Kitano, M.; Nakajima, K.; Kondo, J. N.; Hayashi, S.; Hara, M. *J. Am. Chem. Soc.* **2010**, *132*, 6622–6623.
- (38) Phan, N. T. S.; Le, K. K. A.; Phan, T. D. *Appl. Catal., A* **2010**, *382*, 246–253.
- (39) Ravon, U.; Savonnet, M.; Aguado, S.; Domine, M. E.; Janneau, E.; Farrusseng, D. *Microporous Mesoporous Mater.* **2010**, *129*, 319–329.
- (40) Sebti, S.; Tahir, R.; Nazih, R.; Boulaajaj, S. *Appl. Catal., A* **2001**, *218*, 25–30.
- (41) Deng, M.; Ling, Y.; Xia, B.; Chen, Z.; Zhou, Y.; Liu, X.; Yue, B.; He, H. *Chem.—Eur. J.* **2011**, *17*, 10323–10328.
- (42) Ravon, U.; Domine, M. E.; Gaudillère, C.; Desmartin-Chomel, A.; Farrusseng, D. *New J. Chem.* **2008**, *32*, 937–940.
- (43) Corma, A. *J. Catal.* **2003**, *216*, 298–312.
- (44) Vimont, A.; Goupil, J.-M.; Lavalley, J.-C.; Daturi, M.; Surblé, S.; Serre, C.; Millange, F.; Férey, G.; Audebrand, N. *J. Am. Chem. Soc.* **2006**, *128*, 3218–3227.
- (45) Horcajada, P.; Surblé, S.; Serre, C.; Hong, D. Y.; Seo, Y. K.; Chang, J. S.; Grenèche, J. M.; Margiolaki, L.; Férey, G. *Chem. Commun.* **2007**, 2820–2822.
- (46) Chen, L.; Yang, Y.; Guo, Z.; Jiang, D. *Adv. Mater.* **2011**, *23*, 3149–3154.
- (47) Romano, F.; Linden, A.; Mba, M.; Zonta, C.; Licinia, G. *Adv. Synth. Catal.* **2010**, *352*, 2937–2942.
- (48) Xamena, F. X. L.; Casanova, O.; TAILLEUR, R. G.; Garcia, H.; Corma, H. *J. Catal.* **2008**, *255*, 220–227.
- (49) Alaerts, L.; Séguin, E.; Poelman, H.; Thibault-Starzyk, F.; Jacobs, P. A.; De Vos, D. E. *Chem.—Eur. J.* **2006**, *12*, 7353–7363.
- (50) Sen, R.; Koner, S.; Hazra, D. K.; Helliwell, M.; Mukherjee, M. *Eur. J. Inorg. Chem.* **2011**, 241–248.
- (51) Huang, Y.; Liu, T.; Lin, J.; Lü, J.; Lin, Z.; Cao, R. *Inorg. Chem.* **2011**, *50*, 2191–2198.
- (52) Maksimchuk, N. V.; Timofeev, M. N.; Melgunov, M. S.; Shmakov, A. N.; Chesalov, Yu. A.; Dytsev, D. N.; Fedin, V. P.; Kholdeev, O. A. *J. Catal.* **2008**, *257*, 315–323.
- (53) Kamata, K.; Yonehara, K.; Sumida, Y.; Hirata, K.; Nojima, S.; Mizuno, N. *Angew. Chem., Int. Ed.* **2011**, *50*, 12062–12066.
- (54) Dhakshinamoorthy, A.; Alvaro, M.; Garcia, H. *Chem.—Eur. J.* **2010**, *16*, 8530–8536.
- (55) Dhakshinamoorthy, A.; Alvaro, M.; Garcia, H. *J. Catal.* **2009**, *267*, 1–4.